Journal of
Applied Crystallography
ISSN 0021-8898

Received 14 October 2010
Accepted 22 February 2011

CYCLOPS – a reciprocal-space explorer based on CCD neutron detectors

Bachir Ouladdiaf,[a]* John Archer,[a] John R. Allibon,[a] Philippe Decarpentrie,[a] Marie-Hélène Lemée-Cailleau,[a] Juan Rodríguez-Carvajal,[a] Alan W. Hewat,[a,b] Scott York,[c] Daniel Brau[c] and Garry J. McIntyre[a,d]

[a]Diffraction Group, Institut Laue–Langevin, 6 rue Jules Horowitz, Grenoble 38042, France, [b]NeutronOptics, Grenoble, France, [c]Photonic Science Limited, Robertsbridge, East Sussex TN32 5LA, UK, and [d]Department of Chemistry, University of Durham, South Road, Durham DH1 3LE, UK. Correspondence e-mail: ouladdiaf@ill.eu

The key technical aspects of the multiple CCD diffractometer CYCLOPS (Cylindrical CCD Laue Octagonal Photo Scintillator) at the Institut Laue–Langevin are described. Laue patterns subtending 270° horizontally by 92° vertically are read out in less than 3 s to allow nearly real time exploration of reciprocal space and rapid data collection through phase transitions. The first experiments on the same thermal beam as OrientExpress have exceeded expectations and promise exciting new applications for neutron Laue diffraction.

1. Introduction

The biological Laue diffractometer LADI (Cipriani *et al.*, 1996) and the thermal-neutron Laue diffractometer VIVALDI (Wilkinson *et al.*, 2002; McIntyre *et al.*, 2006) at the Institut Laue–Langevin (ILL) have demonstrated in a spectacular manner the advantages of the Laue technique with a large solid angle of detection. The product of the 8 steradian solid angle of detection together with the wide and intense thermal-neutron waveband yields gains in data-collection efficiency of 10–100 over conventional monochromatic single-crystal diffractometers at the same reactor source. VIVALDI is especially suited for small or weakly scattering crystals, but its application to fast crystallography is limited by the total readout and erasure time of 5 min of its image-plate detector. By contrast, on the CCD-based flat-plate Laue diffractometer OrientExpress (Ouladdiaf *et al.*, 2006), also at the ILL, the 1680 × 1320 pixel image is read out in less than 0.2 s. OrientExpress is used principally for accurate alignment and characterization of single crystals for other experiments with a gain of about 100 in speed compared to conventional photographic film and with similar spatial resolution. The obvious question is why not use CCD detectors in cylindrical geometry to have the principal advantages of both instruments?

Here we describe the most recent addition to the suite of Laue instruments at the ILL. Named CYCLOPS, an acronym for 'Cylindrical CCD Laue Octagonal Photo Scintillator', the instrument is essentially eight copies of the OrientExpress detector rotated to put the longer dimension vertical and arranged in the form of an octagonal cylinder to give a solid angle of detection similar to that of VIVALDI with readout in less than 3 s (Hewat, 2006).

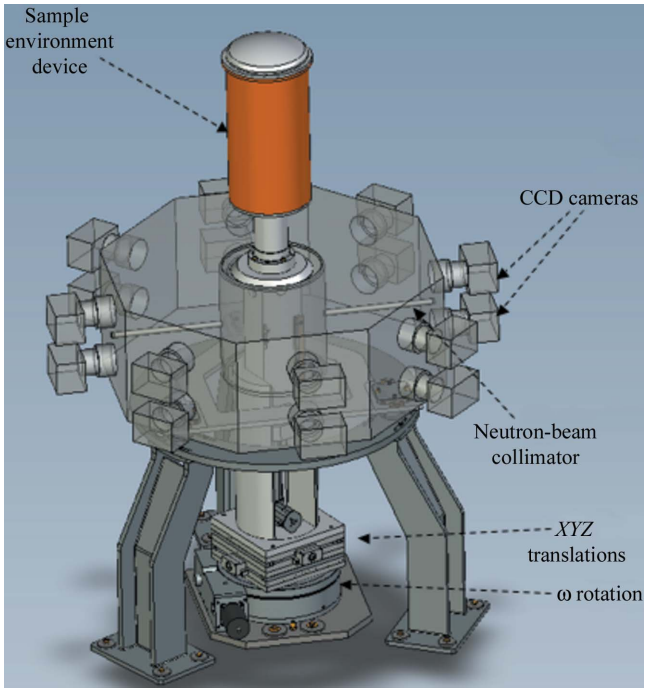

Figure 1
Schematic view of the neutron Laue diffractometer CYCLOPS, showing the full complement of 16 CCD cameras and a cryostat mounted on the sample translation and rotation stage. The incident neutron beam enters *via* the thin tube between the two CCD detectors. The sample is located within the tail of the cryostat at the centre of the octagonal detector housing.

2. CYCLOPS

2.1. Technical aspects

A schematic view of the complete instrument is shown in Fig. 1. The octagonal geometry is maintained by a monolithic octagonal annulus, divided into eight 45° segments. The large-area neutron scintillator behind each inner octagonal face is

Table 1
Technical specifications of CYCLOPS.

Wavelength range (Å)	0.8–5.0
Incident-beam divergence (°)/Å	0.17
Detector height (mm)	412
Detector diameter (mm)	400
Diameter of the sample-environment space (mm)	390
Beam diameter	Variable from 1 to 9 mm
Scintillator	^{6}LiF/ZnS:Ag, 0.210 mm thickness on 1.15 mm Al plate
Pixel size (µm)	0.172 × 0.172
Number of pixels per camera	1200 × 960
Input active area per scintillator (mm)	412 × 165
Intensifier	Ultra-high-resolution Gen 2
Readout speed	10 MHz
Saturation	Approximately 13 000 electrons at minimum gain

viewed *via* two f0.95 close-focus lenses by two high-performance thermoelectrically cooled image-intensified CCD cameras 200 mm apart vertically. The vertical blind regions between octagonal faces are 0.91 mm wide and subtend just 0.24° at the sample position. The incident and transmitted neutron beams pass through the octagonal casing and the centres of one pair of opposing scintillator faces *via* small-diameter tubes without obscuring the view of the scintillators by the cameras.

The neutron scintillators are 0.21 mm-thick AST ND (Applied Scintillation Technologies; http://www.appscintech.com) screens based on ZnS:Ag with ^{6}LiF added to provide reasonably high neutron-capture efficiency. Coupling between the intensifier and the CCD in each camera is *via* a fiber-optic taper that is bonded directly onto the CCD to give maximum transmission and high sensitivity.

The total active scintillator area of 165 × 412 mm (× 8) is rendered as a single image in 8, 12 or 16 bit TIFF format of 7680 × 2400 pixels, each pixel being 172 µm on edge. Integration periods of 1 ms to many minutes and on-chip binning independently in *X* (horizontal direction) and *Y* (vertical direction) are possible. The intensifier gain is fully adjustable *via* software that offers the possibility to optimize the frame rate, resolution, sensitivity, image size and dynamic range for each application. Table 1 summarizes the technical specifications of the instrument.

The modular nature of the octagonal detector facilitates construction and maintenance, with each dual-CCD camera unit being independent mechanically and electronically. This allowed us to begin with just four dual-CCD cameras within our initial budget. Fig. 2 shows the layout of the instrument installed on the H24 thermal guide.

Like OrientExpress, the complete detector, including housing, scintillators, CCDs and associated electronics, was constructed by Photonic Science Ltd (http://photonic-science.co.uk/). Further dual-CCD camera units are being added as funds become available; there are presently six units.

The sample table includes a heavy-duty rotation table, effecting a rotation denoted by ω about the detector vertical axis, below a three-way translation stage. The vertical translation has a total movement of 34 cm, which allows the mounting surface to be raised to the upper level of the detector housing for easy mounting and dismounting of samples and sample environments. The free diameter of 390 mm around the sample, three-times larger than that of VIVALDI, permits a considerably wider range of sample environments, including large pressure cells, furnaces and cryomagnets.

CYCLOPS is presently located at the end of the H24 thermal guide at the position previously occupied by OrientExpress (Ouladdiaf *et al.*, 2006). The latter has been moved 3 m downstream to use the beam transmitted by CYCLOPS.

2.2. Data acquisition and correction

The operation of all dual-CCD cameras is controlled *via* a PC using a customized dialog box in the image-capture and image-analysis software package from Photonic Science Ltd (*PSL*). Parameters that can be modified *via* the dialog box include the intensifier gain, integration time, on-chip binning, offset, flat-field correction file and removal of bright pixels. The exposure of all cameras is synchronized to occur simul-

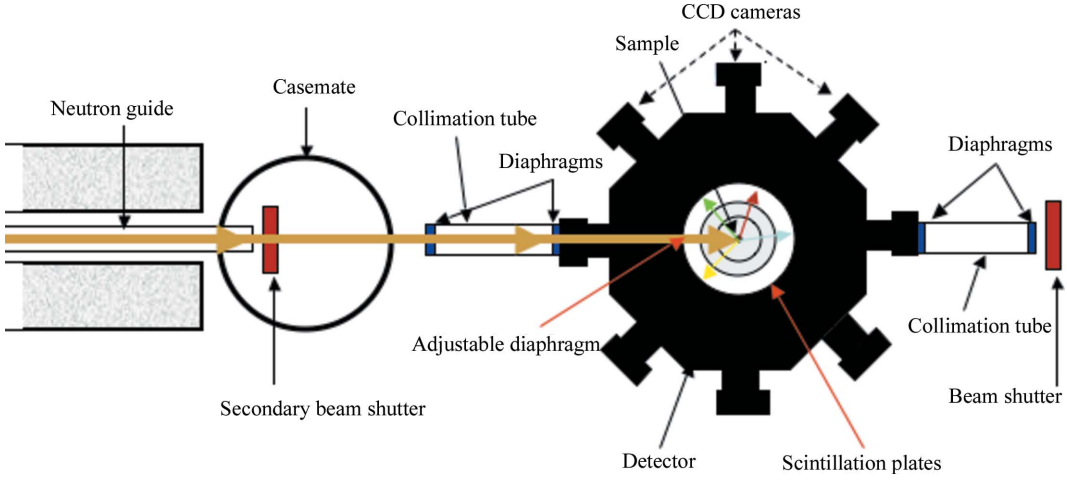

Figure 2
The layout of CYCLOPS installed at the end of the H24 thermal guide at ILL.

taneously, but they transfer their images to the PC serially, where a custom routine in the *PSL* software reconstructs a stitched undistorted image of the diffraction pattern on each octagonal face and then abuts these vertical edge by vertical edge in a single image. The total readout time is ~3 s for six dual camera units.

In routine operation of CYCLOPS, the *PSL* software application runs as a client of the standard ILL diffractometer-control software *MAD*, itself running on a Linux workstation, to permit automated collection and storage of series of Laue patterns at, for example, a number of ω positions at each step of a sequence of temperature settings. More significantly, the short readout time allows frequent readout and updated display during acquisition of a single Laue pattern to give near real time exploration of reciprocal space. The intensifiers and CCDs are calibrated using light from a self-luminous electroluminescent source with the same spectral content as the emission spectrum of the neutron scintillators. The flat-field correction provides an image of spatially uniform intensity to compensate for lens shading, intensifier non-uniformity, and fixed pattern noise from both the fibre optics and the image intensifier. The balancing correction compensates for the natural variation amongst the image intensifiers, to produce an intensity-matched image from all cameras over the whole gain range. The individual images from each camera are distortion corrected by reference to an individual file for each camera. This file is a pixel-by-pixel look-up table, which for each pixel location in the final image identifies where in the raw source image the pixel value should be sampled. Each map file corrects the distortions introduced by the lenses and fibre optics such that the scintillator in front of each camera is imaged with truly square, flat and undistorted geometry.

The ensemble of scintillator, CCD, readout electronics, and algorithms for efficiency correction and stitching together of the two parts of each octagonal face is an integrating detector rather than a quantum counter. It is therefore essential to characterize the gain and point-spread function of the ensemble, and indeed each dual-CCD camera unit, to ensure that correct estimates are made of the true estimated standard deviations in the integrated Laue reflections.

The apparent gain and correlation between neighbouring pixels were calculated from the incoherent scattering recorded from a Plexiglas sphere of 3 mm in diameter following the method described by Wilkinson *et al.* (2009). With a present intensifier gain of 20, all 12 individual CCD cameras in the present configuration are reasonably identical, with a mean apparent gain of 0.79 and point spreads of about 4 pixels vertically and horizontally, after allowance for the mean electronic offset of 101, to give an overall gain of 94.1. The sensitivity was estimated by measuring the integrated intensity in a well resolved Laue spot from a standard ruby crystal (see below) with a ^{3}He single detector, and comparing this with the integrated counts recorded by the CCD camera over the same period of time. This gave 13.93 CCD counts per neutron, and thence a detective quantum efficiency (DQE) of $13.93/(94.1 \times 0.79) = 0.19$. The DQE and resolution are essentially the same as on OrientExpress. Tests of the OrientExpress CCD-like detector on the D9 and D19 four-circle diffractometers, which are located close to the reactor face, indicate that the scintillator has very low γ sensitivity.

2.3. Experimental protocol

The Laue experiment is itself very simple, entailing collection of four to ten diffraction patterns, successive patterns distinguished by a rotation of typically 20 or 30° of the crystal about the detector axis. Studies of phase transitions usually consist of complete experiments at one or two temperatures, and a series of single patterns at one setting of the crystal at small temperature intervals through the transition.

2.4. Data analysis

A single image is produced by *PSL* software with the patterns from the dual-CCD units side by side. The transformation from octagonal geometry to cylindrical geometry is effected by either the *PSL* software application itself or a local plug-in for the general image-manipulation program *ImageJ* (Rasband, 2009; McIntyre & Wilkinson, 2010). As with VIVALDI and LADI, most data from CYCLOPS can then be displayed, indexed and scaled to a common wavelength using interactive programs of the CCP4 Laue suite (Campbell *et al.*, 1998; Helliwell *et al.*, 1989). The reflections are integrated using a two-dimensional version of the three-dimensional minimum-$\sigma(I)/I$ routine of Wilkinson *et al.* (1988), in which the integration boundaries for weak reflections are determined from those observed for nearby strong reflections. It is essential to allow the integration boundary to vary in shape and orientation across the detector surface since the reflection shapes are mostly projections of the crystal shape, which may be strongly anisotropic.

3. First experiments

3.1. Standard ruby sphere

Ruby spheres with diameters of 1, 2 and 3 mm from Arcanum Corporation are used on a number of monochromatic diffractometers at the ILL for instrument alignment and determination of the wavelength and instrumental offsets. These rubies are of the same material as the 0.15 mm-diameter spheres of the certified standard reference material (SRM 1990; Wong-Ng *et al.*, 2001). The strong scattering and spherical form permits rapid determination of reflection centroids. The same characteristics are also advantageous on thermal Laue instruments, giving clean Laue patterns with sharp elliptical spots for frequent short full data collections to monitor the incident flux and spectrum, and to determine various detector parameters. The sample volume is considerably larger than that of most samples studied on VIVALDI and generally leads to difficulties in correcting for extinction; nevertheless the samples are very useful calibrating standards.

Fig. 3 shows one Laue pattern transformed to cylindrical geometry, obtained for the five dual-CCD units that were present on CYCLOPS at the time of measurement, after correction for distortion and stitching together of the pairs of

Table 2
Fractional atomic coordinates and anisotropic displacement parameters (Å^2) from a 9 min data collection from a 3 mm ruby sphere.

Atom	x	y	z	B_{11}	B_{22}	B_{33}	B_{23}	B_{13}	B_{12}
Al	0	0	0.3521 (2)	0.14 (9)	0.14 (9)	0.14 (10)	0	0	−0.18 (4)
O	0.3076 (4)	0	0.25	0.04 (4)	0.31 (7)	0.11 (7)	0.07 (3)	0.02 (1)	−0.10 (3)

RF2 (%)	11.6
RF2w (%)	12.4
RF (%)	8.0
χ^2	1.7

The form of the temperature factor is $\exp(-1(B_{11}h^2a^{*2} + \cdots + 2B_{23}hb^*kc^* + \cdots))$.

patterns from each unit. The indexing of the patterns was performed by the program *LAUEGEN* from the CCP4 Laue suite, using the lattice parameters a = 4.761 and c = 13.002 Å determined from a monochromatic diffraction experiment. Nine such patterns at different positions in crystal rotation ω were recorded, each for 1 min, and analysed to extract integrated intensities normalized to a common wavelength. A total of 1082 reflections with 181 independent reflections were measured with an R internal for equivalent reflections of 11.7%. The main results show good agreement between refined predicted and observed spot positions. The crystal structure was refined against the observed structure factors using *sflsq* of the Cambridge Crystallographic Subroutine Library (Matthewman *et al.*, 1982) and the *FullProf* suite (Rodríguez-Carvajal, 1993). The refined fractional atomic coordinates, anisotropic displacement parameters and conventional R factors are given in Table 2. Not surprisingly, extinction is rather severe for some reflections, but is reasonably well modelled by a Becker & Coppens (1974, 1975) type 1 mode with a Lorentzian distribution of domain orientations.

3.2. Weakly scattering, large unit cells

One challenge for CYCLOPS is its capability to measure a large-unit-cell organic compound containing hydrogen. Fig. 4 shows the Laue pattern from a 6 mm^3 single crystal of the hydrated enantiopure benzocyclotrimer $C_{30}H_{42}O_{3.2}\cdot 5H_2O$ (Fabris *et al.*, 2010). The compound is hexagonal with space group $P6_522$ and lattice parameters a = 10.91 and c = 81.73 Å, leading to a primitive cell volume of 8424 Å^3. As one can see from Fig. 4, a very good pattern can be obtained in 2 h of measuring time. The inset shows the line profile along the selected arc of reflections, indicating a good spatial resolution of neighbouring reflections away from the principal planes.

3.3. Ferroelastic transition in α-$CuSb_2O_6$

The third example concerns the study of the twinning and detwinning mechanism in $CuSb_2O_6$ (Prokofiev *et al.*, 2003). At high temperature, α-$CuSb_2O_6$ has a tetragonal structure ($a \simeq 4.6$, $c \simeq 9.20$ Å, $P4_2/mnm$) and forms square-planar Cu^{2+} lattices parallel to the ab plane, separated along the c axis by two layers of diamagnetic ions. Below 380 K, it exhibits a monoclinic distortion ($a \simeq b \simeq 4.6$, $c \simeq 9.15$ Å, $P2_1/n$ with $\beta \simeq 91^\circ$). When additional antiferromagnetic next-neighbour interactions are present *via* the diagonal of the Cu square, the system is frustrated. Below 49 K quasi-one-dimensional Heisenberg behaviour is reported from the susceptibility (Gibson *et al.*, 2004). Additional three-dimensional long-range antiferromagnetic order is observed below 8.6 K with a propagation vector $\mathbf{k} = (\frac{1}{2}\ 0\ \frac{1}{2})$. The ordered moment of Cu atoms determined from the neutron diffraction experiment is about 0.5 μ_B (μ_B being the Bohr magneton).

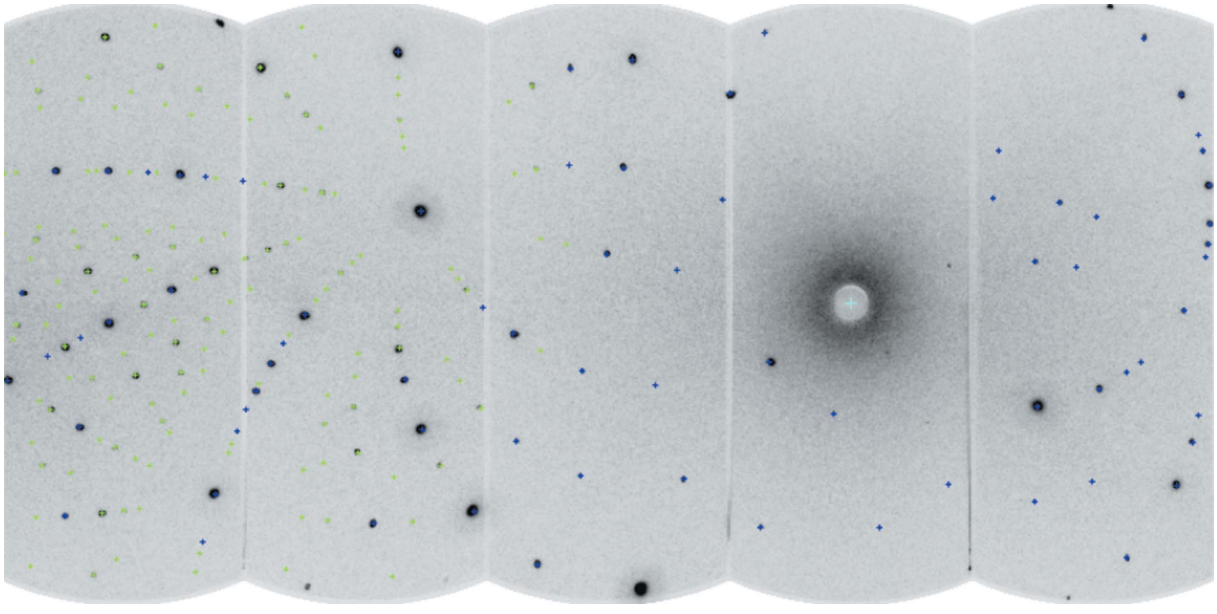

Figure 3
Laue diffraction pattern from a 3 mm-diameter standard ruby crystal seen from the sample taken in 60 s exposure time. In this configuration of five dual-CCD camera units, the incident neutron beam exits through the hole in the centre of the fourth unit.

The tetragonal crystal we used is already twinned owing to the particular metrics ($c \simeq 2a$) that give rise to a pseudo-cubic subcell (Prokofiev *et al.*, 2003). The twin laws are $\langle 100 \rangle_{90^\circ}$, $\langle 201 \rangle_{180^\circ}$ and $\langle 221 \rangle_{120^\circ}$, in which the indices correspond to equivalent direct real space lattice directions (twin axes) and the subscript represents the rotation angle around the twin axis. When the compound goes through the tetragonal-to-monoclinic phase transition at 380 K, the individual components become further twinned because of the symmetry elements lost on going to the monoclinic subgroup. A Laue diffraction experiment at high temperature was performed on CYCLOPS using a standard ILL cryofurnace, in order to identify and to understand the twinning mechanism that takes place at the structural transition. Fig. 5 shows the Laue pattern collected at 400 K, *i.e.* above the structural transition, and corresponds to a twinned crystal of the tetragonal phase. Upon cooling, the Laue spots split when going through the structural transition. The inset of Fig. 5 shows the variation with temperature of the pattern near the prominent Laue spot composed by the reflections of the type {200}/{102}/{110}. Each pattern was collected in 1 min. The strong spot in the tetragonal phase splits into four visible spots with different intensities in the monoclinic phase, indicating several twin domains with different populations. The additional twin laws appearing in the monoclinic phase correspond to the fourfold axis $\langle 001 \rangle_{90^\circ}$, which is oriented in different directions in the twinned tetragonal phase. Furthermore, long exposure patterns (2 h) measured below 8 K allow observation of very weak magnetic reflections associated with the antiferromagnetic ordering of the small Cu moments.

4. Discussion and conclusion

The first results obtained with CYCLOPS during commissioning have exceeded our expectations. Indeed, owing to its fast readout and low γ sensitivity, Laue diffraction patterns with large solid angle are now measurable within several seconds. A complete structure determination for a favourable sample can therefore be achieved in just a few minutes. As shown in the above examples, CYCLOPS provides a unique instrument for real-time surveys of large volumes of reciprocal space under various conditions of temperature, pressure and magnetic field. CYCLOPS is ideal to follow changes in scattering in near real time from magnetic materials as the temperature and magnetic field are varied. Structural and magnetic phase transitions as well as incommensurate structures can be investigated.

Many modern materials exhibit specific properties because of strong intrinsic anisotropy. Examples include thermoelectric materials, fast ionic conductors, permanent magnets, high-critical-temperature superconductors, giant magnetoresistors and shape-memory alloys. The development of materials with strong preferred crystal orientation associated with intrinsic anisotropy of the physical properties is crucial to optimize the macroscopic properties that are used in real devices. Texture can be obtained through uniaxial pressure,

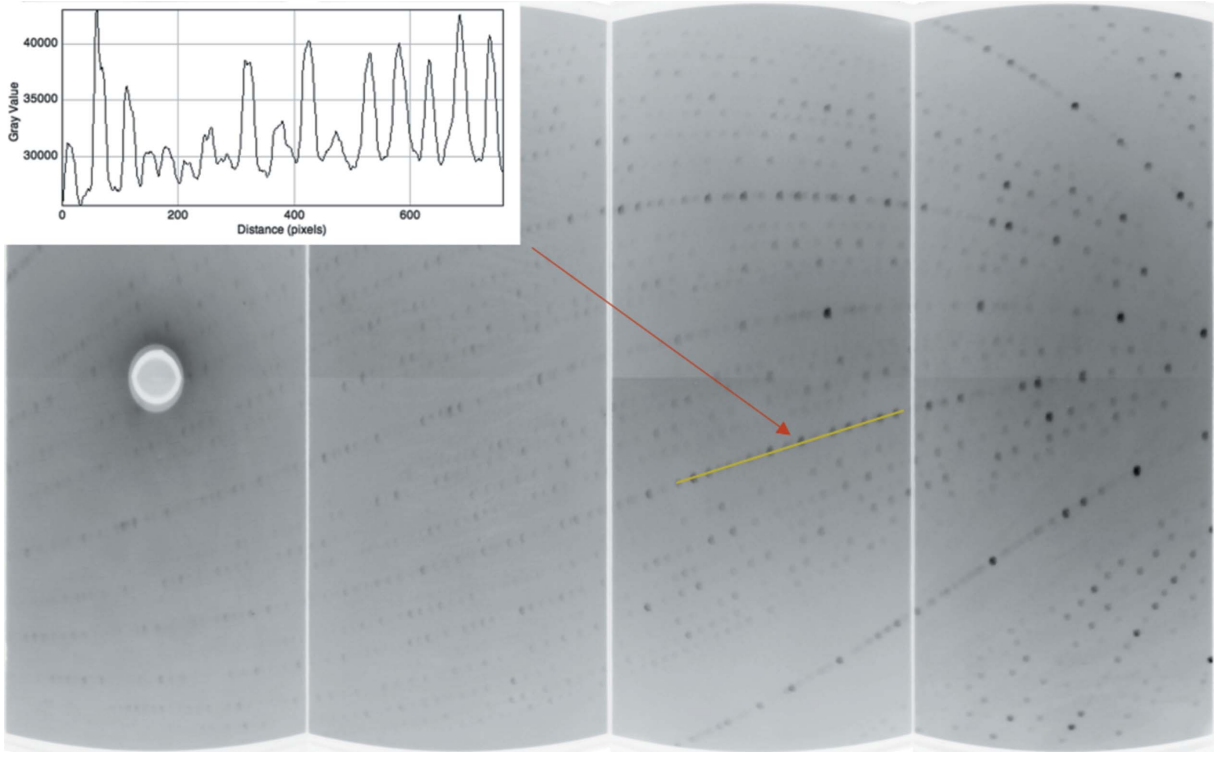

Figure 4
A 2 h exposure from a 6 mm^3 crystal of $C_{30}H_{42}O_{3.2}\cdot 5H_2O$ taken with the initial configuration of four dual-CCD camera units where the incident neutron beam enters through the hole in the left-most unit. The inset shows the line profile along the selected arc of reflections.

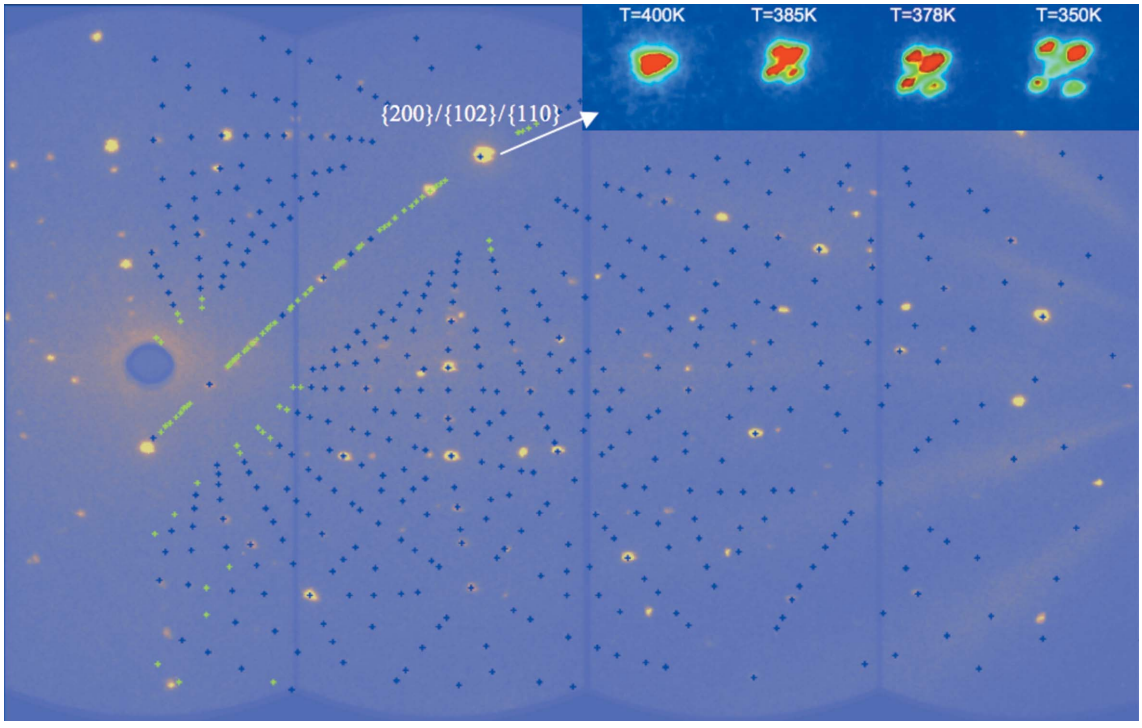

Figure 5
Observed and indexed pattern from a crystal of $CuSb_2O_6$ at 400 K in the tetragonal phase, measured in 60 s using the initial configuration. The inset shows the temperature dependence of the peak shape of the {200}/{102}/{110} composite spot of the tetragonal phase on crossing the structural transition to the monoclinic phase.

magnetic field *etc.*; however, the microscopic mechanism for the development for such texture remains largely unknown owing to the lack of bulk measurement capabilities. This is where CYCLOPS can play an important role by following changes of texture under *in situ* external mechanical, magnetic and thermal loading.

Owing to the large solid angle and low background of CYCLOPS, diffuse scattering due to structural fluctuations and disorder can also be studied. The fast readout allows *in situ* experiments and thermodiffractometry now becomes possible on single crystals with similar time resolution to that with powder samples.

We are very grateful for partial funding of this project from the UK EPSRC. We thank S. A. Mason, M. Enderle, C. Zonta and A. V. Prokofiev for providing the crystals.

References

Becker, P. J. & Coppens, P. (1974). *Acta Cryst.* A**30**, 129–147.
Becker, P. J. & Coppens, P. (1975). *Acta Cryst.* A**31**, 417–425.
Campbell, J. W., Hao, Q., Harding, M. M., Nguti, N. D. & Wilkinson, C. (1998). *J. Appl. Cryst.* **31**, 496–502.
Cipriani, F., Castagna, J. C., Wilkinson, C., Oleinek, P. & Lehmann, M. S. (1996). *J. Neutron Res.* **4**, 79–85.
Fabris, F., De Lucchi, O., Nardini, I., Crisma, M., Mazzanti, A., Mason, S. A., Lemée-Cailleau, M. H. & Zonta, C. (2010). Personal communication.
Gibson, B., Kremer, R. K., Prokofie, A. V., Assmus, W. & Ouladdiaf, B. (2004). *J. Magn. Magn. Mater.* **272–276**, 927–928.
Helliwell, J. R., Habash, J., Cruickshank, D. W. J., Harding, M. M., Greenhough, T. J., Campbell, J. W., Clifton, I. J., Elder, M., Machin, P. A., Papiz, M. Z. & Zurek, S. (1989). *J. Appl. Cryst.* **22**, 483–497.
Hewat, A. W. (2006). *Physica B*, **385–386**, pp. 979–984.
Matthewman, J. C., Thompson, P. & Brown, P. J. (1982). *J. Appl. Cryst.* **15**, 167–173.
McIntyre, G. J., Lemée-Cailleau, M.-H. & Wilkinson, C. (2006). *Physica B*, **385–386**, 1055–1058.
McIntyre, G. J. & Wilkinson, C. (2010). Personal communication.
Ouladdiaf, B., Archer, J., McIntyre, G. J., Hewat, A. W., Brau, D. & York, S. (2006). *Physica B*, **385–386**, 1052–1055.
Prokofiev, A. V., Ritter, F., Assmus, W., Gibson, B. J. & Kremer, R. K. (2003). *J. Crys. Growth*, **247**, 457–466.
Rasband, W. S. (2009). *ImageJ*. National Institutes of Health, Bethesda, Maryland, USA, http://rsb.info.nih.gov/ij/.
Rodríguez-Carvajal, J. (1993). *Physica B*, **192**, 55–69.
Wilkinson, C., Cowan, J. A., Myles, D. A. A., Cipriani, F. & McIntyre, G. J. (2002). *Neutron News*, **13**(1), 37–41.
Wilkinson, C., Khamis, H. W., Stansfield, R. F. D. & McIntyre, G. J. (1988). *J. Appl. Cryst.* **21**, 471–478.
Wilkinson, C., Lehmann, M. S., Meilleur, F., Blakeley, M. P., Myles, D. A. A., Vogelmeier, S., Thoms, M., Walsh, M. & McIntyre, G. J. (2009). *J. Appl. Cryst.* **42**, 749–757.
Wong-Ng, W., Siegrist, T., DeTitta, G. D., Finger, L. W., Evans, H. T., Gabe, E. J., Enright, G. D., Armstrong, J. T., Levenson, M., Cook, L. P. & Hubbard, C. R. (2001). *J. Res. Natl Inst. Stand. Technol.* **106**, 1071–1094.